science, engineering and health studies

Research Article

Science, Engineering and Health Studies
https://lio1.tci-thaijo.org/index.php/sehs
ISSN (Online): 2630-0087

Improved ultra-short-term pulse rate variability using hair detection and majority vote in subintervals

Panupong Sunkom[1], Denchai Worasawate[1], Chadchai Srisurangkul[2], and Minoru Nakayama[3]*

[1] Department of Electrical Engineering, Faculty of Engineering, Kasetsart University, Bangkok 10900, Thailand
[2] National Metal and Materials Technology Center, National Science and Technology Development Agency, Pathum Thani 12120, Thailand
[3] School of Engineering, Tokyo Institute of Technology, Tokyo 152-8550, Japan

***Corresponding author**: Denchai Worasawate
denchai.w@ku.th*

***Received**: 5 October 2023*
***Revised**: 11 September 2024*
***Accepted**: 17 September 2024*
***Published**: 31 December 2024*

***Citation**: Sunkom, P., Worasawate, D., Srisurangkul, C., and Nakayama, M. (2024). Improved ultra-short-term pulse rate variability using hair detection and majority vote in subintervals. Science, Engineering and Health Studies, 18, 24040012.*

ABSTRACT

Remote photoplethysmography (rPPG) is a non-contact method for extracting pulse signal from a region of interest (ROI) in a human facial video. This technique enables researchers to remotely measure both heart rate and pulse rate variability (PRV). However, when the forehead is used as the ROI for rPPG signal extraction, hair can obscure parts of the skin, and changes in ambient lighting may introduce spurious frequency spikes, which degrade the rPPG signal and PRV accuracy. This paper proposed a method to improve ultra-short-term PRV derived from the rPPG signal using the forehead ROI. The approach incorporated a hair detection algorithm to extract the rPPG signal from skin areas, excluding regions covered by hair. In addition, a majority voting mechanism was applied to subintervals to determine the optimal passband frequency for a bandpass filter, effectively eliminating spurious frequencies. The ultra-short-term PRV was then computed from the refined rPPG signal. Results show that the mean absolute error of the ultra-short-term PRV was improved for most subjects compared to the mean absolute error obtained via the conventional method.

Keywords: remote photoplethysmography; hair detection; time domain ultra-short-term pulse rate variability

1. INTRODUCTION

Heart rate variability (HRV) is a measure of an individual's health, reflecting changes in the time intervals between successive heartbeats. It serves as an important indicator of autonomic nervous system (ANS) activity (McCraty and Shaffer, 2015). Typically, HRV is measured using medical devices such as electrocardiograms (ECGs). However, the complexity and inconvenience of the ECG acquisition process can lead to potential errors (Bolanos et al., 2006). To overcome these challenges, the photoplethysmography (PPG) signal—captured using a pulse oximeter attached to a subject's finger to measure the blood volume pulse (BVP)—has been proposed as an alternative (Peng et al., 2015). HRV derived from the PPG signal is referred to as pulse rate variability (PRV). Several studies have demonstrated that PRV obtained from the PPG signal can effectively serve as a surrogate for HRV derived from ECG signal (Aimie-Salleh et al., 2020; Pinheiro et al., 2016; Vescio et al., 2018). PRV is calculated by analyzing the pulse-to-pulse interval (PPI) within the PPG signal.

Attaching a pulse oximeter to a subject's finger can be inconvenient for acquiring PRV during activities involving hand movement, such as driving. To address this limitation, remote photoplethysmography (rPPG) has been introduced as a non-contact method for capturing the

blood volume pulse (BVP) component. Instead of relying on signals from contact-based medical devices, rPPG extract BVP from a region of interest (ROI) in a human facial video. For effective rPPG signal acquisition, careful selection of the ROI is crucial to ensure a strong BVP component. Kumar et al. (2015) demonstrated that the forehead and cheeks are optimal regions for detecting the BVP component. Over the years, various techniques have been developed to extract the rPPG signal from facial videos. These include blind source separation (BSS) methods (Lewandowska et al., 2011; Panigrahi and Sharma, 2022; Poh et al., 2010) and model-based approaches such as CHROM (de Haan and Jeanne, 2013), POS (Wang et al., 2017), and modified POS (Ryu et al., 2021).

Previous studies used rPPG signal to extract PRV from human facial videos as a non-contact alternative to traditional contact-based medical devices. The findings from these studies indicate that PRV derived from rPPG signal is comparable to that obtained from medical devices (Gudi et al., 2020; Yu et al., 2021). Recently, Finžgar and Podržaj (2020) explored the use of ultra-short-term PRV, defined as PRV obtained from signals lasting less than five minutes. Their experimental results, based on recording durations ranging from 10 to 60 s, showed that the agreement between the ultra-short-term PRV derived from rPPG and PPG signals improves with longer recording durations.

Sunkom et al. (2023) proposed a method to improve heart rate (HR) measurements derived from rPPG signal using a 10-s interval extracted from the forehead ROI with the modified POS method (Ryu et al., 2021). This method divides the forehead ROI into 24 small areas and applies a hair detection algorithm to exclude regions covered by hair. Additionally, a majority voting mechanism is employed in subintervals to identify the optimal passband frequency for filtering the rPPG signal. The results demonstrate that HR measurements are improved by excluding hair-covered areas and using the majority voting to eliminate spurious frequencies caused by changes in ambient lighting.

This study extends the work of Sunkom et al. (2023) by applying their algorithms to enhance ultra-short-term PRV derived from the rPPG signals. To achieve this, certain parameters and processes within the algorithm have been adjusted and simplified to reduce complexity. This paper provided an overview of the original algorithm proposed by Sunkom et al. (2023), describes the modifications made, and demonstrated how these adjustments improve the accuracy of ultra-short-term PRV.

2. MATERIALS AND METHODS

2.1 Materials

This study utilized the UBFC-RPPG public dataset (Bobbia et al., 2019), which contains one-minute video recordings of human faces engaged in a mathematical game. The videos were captured with a Logitech C920 HD Pro webcam, at a frame rate of 30 frames per second (fps) and a resolution of 640 × 480 pixels, with subjects positioned approximately one meter from the webcam. The dataset also includes PPG signals recorded with a CMS50E pulse oximeter, which serve as the ground truth for comparison with the results of the proposed method.

For the experiments, seven videos were selected from the dataset, focusing on subjects whose hair partially covered their forehead areas. The selected videos correspond to subject IDs #5, #10, #14, #23, #30, #32, and #35. Figure 1 shows the facial images of these subjects along with their ID numbers.

2.2 Methods

An overview of the proposed method is shown in Figure 2. This method builds on the approach described by Sunkom et al. (2023), with modifications to certain parameters and processes to facilitate ultra-short-term PRV calculation while reducing overall complexity. The method consists of five main components. Detail descriptions of each component are provided below.

2.2.1 Forehead ROI extraction

To identify and extract the ROI on the subject's face, a face detection model was used to detect and track the face. In this study, the MediaPipe Face Mesh model (Kartynnik et al., 2019) was employed to locate and generate 3D facial landmark points. The ROI was then extracted by selecting specific facial landmark points. Based on experiments conducted by Sunkom et al. (2023), two types of forehead ROIs were utilized for ultra-short-term PRV calculation: the entire forehead ROI and smaller areas within the forehead ROI. The PRVs obtained from these two types were compared.

The entire forehead ROI, commonly used in various studies, is a conventional region for tPPG signal extraction (Lewandowska et al., 2011; Pourbemany et al., 2021; Sanyal and Nundy, 2018). In this study, the entire forehead ROI was defined by the facial landmark points 9, 10, 66, 67, 103, 104, 105, 107, 109, 296, 297, 332, 333, 334, 336, and 338, as displayed in Figure 3a. However, this ROI can be partially covered by hair, which may affect the quality of the rPPG signal, as depicted in Figure 3b.

To address this issue, the entire forehead ROI was divided into 24 smaller triangular areas, as detailed in Figure 4a. Figure 4b illustrates how these areas are positioned on the subject's face. The triangular areas were classified into hair and skin regions, with only the skin regions being used for rPPG signal extraction.

2.2.2 Raw RGB color signal extraction and hair detection algorithm

The raw RGB color signals for each area were extracted using the spatial average technique, which calculated the average values of red, green, and blue within each video frame, as illustrated in Equation 1:

$$\boldsymbol{C}^{*}_{i,j}(t) = \frac{\sum_{k=1}^{K} \boldsymbol{c}^{*}_{i,k,j}(t)}{K}, \; i \in \{\mathrm{R,G,B}\} \qquad (1)$$

where $\boldsymbol{C}^{*}_{i,j}(t)$ is the raw RGB color signal of the j^{th} area of the forehead ROI, $\boldsymbol{c}^{*}_{i,k,j}(t)$ is the raw RGB color signal of the k^{th} pixel in the j^{th} area, and K is the number of pixels in the j^{th} area.

For the entire forehead ROI, only a single raw RGB color signal was extracted, combining the color information from both hair and skin pixels. In contrast, the smaller areas within the forehead ROI consisted of 24 distinct regions, resulting in the extraction of 24 separate raw RGB color signals.

Figure 1. Facial images and ID numbers of the selected subjects for this study

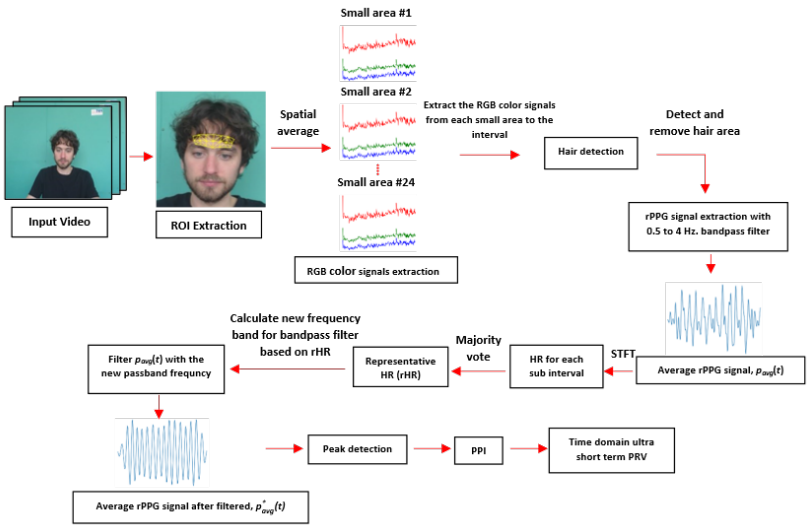

Figure 2. Overview of the proposed method used to improve ultra-short-term PRV

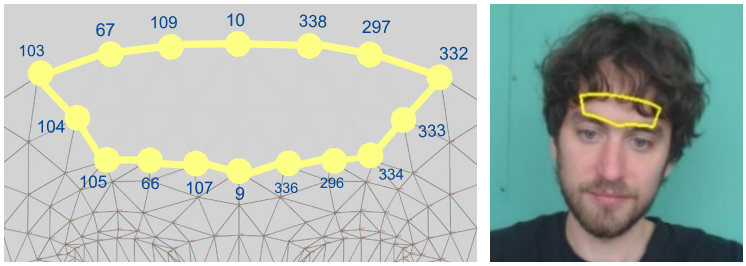

(a) (b)

Figure 3. Entire forehead ROI; (a) facial landmark points used to define the ROI, (b) visualization of the ROI on the subject's face

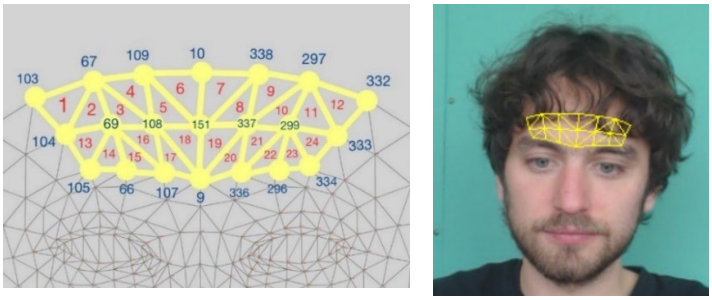

(a) (b)

Figure 4. Small areas within the forehead ROI; (a) facial landmark points used to define the ROI, (b) visualization of the ROI on the subject's face

In the study by Sunkom et al. (2023), 10-s intervals (300 samples) of the raw RGB color signals were used for HR calculation. However, to improve the alignment between the ultra-short-term PRV derived from the rPPG signal and the ground truth PRV obtained from the PPG signal (Finžgar and Podržaj, 2020), this study uses a longer signal duration. Specifically, a 20-s interval (600 samples) was selected. This interval is updated every sec by removing the initial 1-s segment (30 samples) and appending a new 1-s segment (30 samples) at the end, as illustrated in Figure 5. The process continues until the video ends.

For the smaller areas within the forehead ROI, the hair detection algorithm described by Sunkom et al. (2023) was applied to the 20-s signal of the 24 areas. The algorithm begins by calculating the average green color signal for each area, and identifying the area with the highest average green value. It then normalizes the green color values for each area and classifies them as either containing hair or not based on these normalized values. Areas marked as 'No' are identified as skin region, and used to rPPG signal extraction in subsequent processing. Conversely, areas marked as 'Yes' (indicating the presence of hair) are excluded from further analysis. Additional details of the hair detection algorithm can be found in the original study by Sunkom et al. (2023).

2.2.3 rPPG signal extraction

The modified POS, as outlined by Ryu et al. (2021), was used to extract rPPG signals. This method involves projecting the RGB signals onto the 'plane-orthogonal-to-skin' (POS) using Equation 2:

$$S(t) = P \cdot C_{RGB,n}(t) \tag{2}$$

where $S(t)$ is the projected signal matrix with dimensions $2 \times N_f$ (N_f represents the length of the defined interval), P is the 2×3 projection matrix given by Ryu et al. (2021), and $C_{RGB,n}(t) = [C_{R,n}(t) \quad C_{G,n}(t) \quad C_{B,n}(t)]^T$ denotes the temporally normalized RGB color matrix with dimensions $3 \times N_f$ from the n^{th} skin area. $C_{i,n}(t)$ are computed as follows:

$$C_{i,n}(t) = \frac{C^*_{i,n}(t)}{\mu\left(C^*_{i,n}(t)\right)}, \; i \in \{R,G,B\} \tag{3}$$

where $C^*_{i,n}(t)$ is the raw color signals, $\mu(\bullet)$ denotes the operator used to compute the average value, and the subscript n indicates the specific skin area.

The rPPG signal from each skin area, denoted as $p_n(t)$, is calculated using:

$$p_n(t) = BP[\, S_1(t) + \alpha \cdot S_2(t)]_{f_{low}}^{f_{high}} \;\text{ with }\; \alpha = \frac{\sigma(S_1(t))}{\sigma(S_2(t))} \tag{4}$$

where $S_i(t)$ is the i^{th} row of $S(t)$, and $\sigma(\bullet)$ represents the standard deviation operator. The operator $BP[\bullet]_{f_{low}}^{f_{high}}$ is a signal filtering process using a third-order bandpass filter with a passband frequency of f_{low} to f_{high}. In this study, f_{low} was set to 0.5 Hz and f_{high} to 4Hz, corresponding to an HR range of 30 to 240 beats per min (BPM). This filtering step captures the dominant frequency components of the BVP while effectively reducing noise.

Finally, the mean rPPG signal, $\boldsymbol{p}_{avg}(t)$, is computed by averaging the rPPG signals from all skin areas:

$$p_{avg}(t) = \frac{\sum_{n=1}^{N} p_n(t)}{N} \tag{5}$$

where N is the number of skin areas.

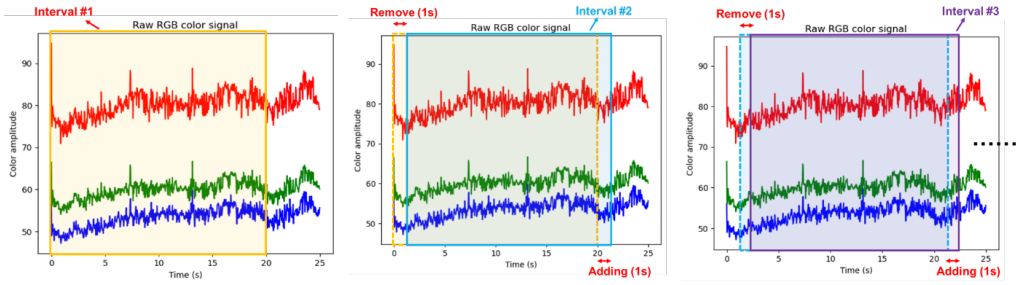

(a) (b) (c)

Figure 5. The details of the divided interval and the update process; (a) initial interval with a duration of 20 s, (b) second interval generated through the update process, and (c) third interval produced by continuing the update process
Note: This iterative update continues until all data from the facial video has been processed.

2.2.4 Identification of the optimal rPPG frequency band using the majority vote in subintervals

The majority vote in subintervals method used in this study has been modified from the original approach proposed by Sunkom et al. (2023) to reduce computational complexity.

The algorithm identifies the optimal frequency band for the bandpass filter by determining the representative heart rate (rHR) of the majority group, derived from the majority vote in subintervals. To determine the majority group, the mean rPPG signal, pavg(t), obtained from Section C, was divided into subintervals. The short-time Fourier transform (STFT) was applied to each subinterval to identify the frequency component with the highest amplitude. The HR for each subinterval was set to $60 \cdot f_{max}$, where f_{max} is the frequency component with the highest amplitude.

The HRs from each subinterval were grouped into multiple intervals of equal size, starting with a range of 5 BPM, e.g., 80 to 85 BPM ($80 \le HR < 85$) and 85 to 90 BPM ($85 \le HR < 90$). The number of HRs within each group was counted, and the group with the highest count was identified as the majority group. The rHR was then calculated as the midpoint of this

majority group. For additional details on the majority vote algorithm, refer to Sunkom et al. (2023).

In this study, the STFT parameters were set as follows: nperseg = 180 (6 s), noverlap = 165, and nfft = 1800. These settings extend the subinterval length from 3 to 6 s compared to Sunkom et al. (2023) and update each subinterval by shifting 0.5 s. This adjustment provides a improved frequency resolution for HR calculation in subintervals. With these STFT settings, the 20-s interval of $\boldsymbol{p}_{avg}(t)$ is divided into 29 subintervals. Figure 6 illustrates the STFT settings used in this study.

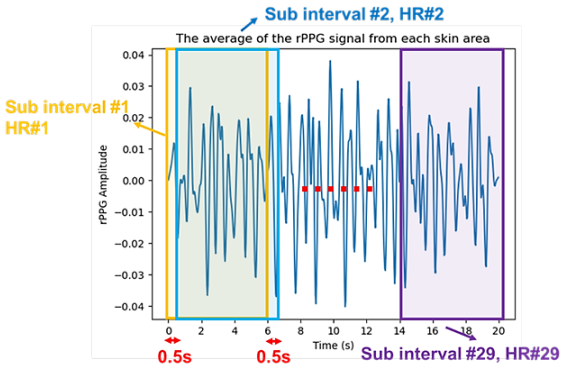

Figure 6. The details of the STFT setting used in this study

Next, the optimal frequency band for the bandpass filter is determined based on the rHR using the following formulas: $f_{\text{low}} = \frac{0.7 \times \text{rHR}}{60}$, $f_{\text{high}} = \frac{1.3 \times \text{rHR}}{60}$. The computational complexity for obtaining the optimal average rPPG signal, denoted as $p^{*}_{avg}(t)$, is reduced compared to the method used in described Sunkom et al. (2023). This is achieved by directly applying a bandpass filter with f_{low} and f_{high}, to $p_{avg}(t)$.

2.2.5 Ultra-short-term PRV calculation

In this study, the Python package Neurokit2 (Makowski et al., 2021) was used to compute time domain PRV features directly from the rPPG signal. The features included: the average of PPI (meanPP), the root mean square of successive differences between adjacent PPIs (RMSSD), the standard deviation of PPI (SDPP), and the standard deviation of successive differences between adjacent PPIs (SDSD).

These PRV features were then calculated from two sources: the rPPG signal obtained from the entire forehead ROI, representing the results of the conventional method, and the rPPG signal derived from the small areas within the forehead ROI, incorporating hair detection and the majority vote in subintervals, representing the results of the proposed method. Both sets of results were compared with the PRV derived from the ground truth PPG.

3. RESULTS AND DISCUSSION

In this study, the mean absolute error (MAE) was used to evaluate the differences between the PRV results obtained from the experiments and the ground truth PPG, as shown in Equation 6. Lower MAE values indicate a closer alignment with the ground truth.

$$\text{MAE} = \frac{\sum_{k=1}^{K} \left| \text{Data}_{gt,k} - \text{Data}_{re,k} \right|}{K} \quad (6)$$

where K is the number of data points, $\text{Data}_{gt,k}$ is the k^{th} ground truth data point, and $\text{Data}_{re,k}$ is the k^{th} experiment data point.

The MAE is calculated for each 10-s interval of the PRV features and updated every second throughout the entire video. The mean and standard deviation of the MAE for both the conventional and proposed methods were then computed, and the data are presented in Tables 1–4.

Table 1. MeanPP results

Subject ID	MAE±SD (ms)	
	Conventional method	Proposed method
#5	74.50±26.78	2.18±0.63
#10	43.32±12.68	8.16±4.97
#14	10.07±7.71	3.63±0.81
#23	28.51±18.52	4.12±0.82
#30	63.56±43.11	16.63±5.31
#32	50.14±53.53	63.97±141.56
#35	1.48±0.51	1.51±0.41

Table 2. SDPP results

Subject	MAE±SD (ms)	
	Conventional method	Proposed method
#5	181.77±51.21	6.95±2.03
#10	98.39±20.15	20.59±10.87
#14	31.70±21.68	19.68±5.48
#23	50.88±25.65	38.13±4.24
#30	148.32±69.17	37.94±16.81
#32	113.80±83.53	24.83±44.95
#35	6.16±2.94	5.63±2.70

Table 3. RMSSD results

Subject	MAE±Std (ms)	
	Conventional method	Proposed method
#5	284.39±68.20	15.59±2.87
#10	161.42±47.60	30.61±12.92
#14	69.70±37.41	49.43±10.21
#23	54.51±19.69	85.13±9.66
#30	245.77±118.48	51.76±25.14
#32	154.51±109.06	39.28±57.65
#35	16.38±10.96	12.80±7.43

Table 4. SDSD results

Subject	MAE±SD (ms)	
	Conventional method	Proposed method
#5	238.92±69.70	15.87±2.94
#10	164.17±48.67	31.06±13.08
#14	71.32±38.36	50.41±10.42
#23	55.73±20.15	87.43±10.02
#30	250.72±121.14	52.63±25.51
#32	157.49±111.65	40.72±60.45
#35	16.67±11.21	12.98±7.54

For the meanPP, the MAEs for five of the seven subjects—specifically, subjects #5, #10, #14, #23, and #30—showed improvement, as detailed in Table 1. This improvement is primarily due to the use of the majority vote in subintervals to determine the optimal passband frequency for the bandpass filter. Figure 7 compares the ground truth PPG with the rPPG signals obtained from both the conventional and proposed methods. As illustrated in Figure 7a, the rPPG signal derived using the conventional method is excessively noisy, leading to inaccurate detection of positive peak indices even after applying a 0.5 to 4 Hz bandpass filter. This noise leads to errors in the calculation of PPIs. In contrast, Figure 7b demonstrates the significant enhanced quality of the rPPG signal obtained using the proposed method. This enhancement enables the peak detection algorithm to accurately identify the indices of positive peaks, resulting in more reliable measurements of PPIs.

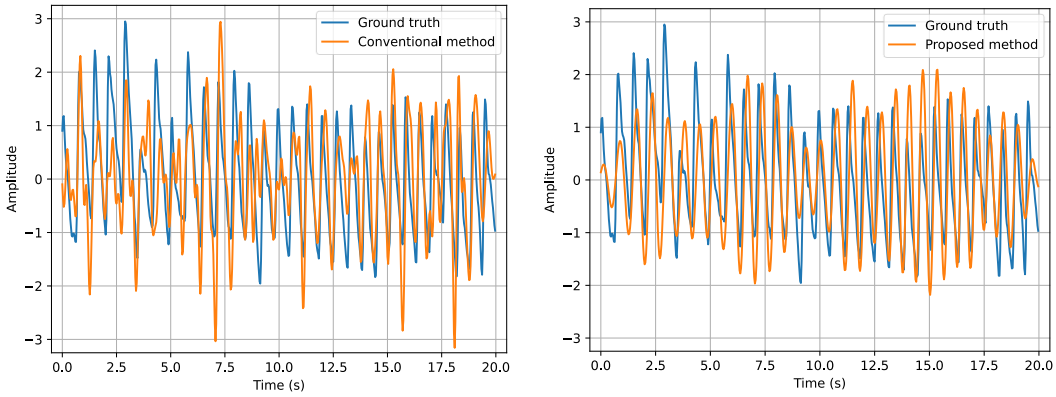

(a) (b)

Figure 7. Comparison of the rPPG signal acquired using each method with the ground truth PPG from the same interval; (a) the rPPG signal acquired using the conventional method versus ground truth PPG, and (b) the rPPG signal acquired using the proposed method versus the ground truth PPG

However, the results for subject #32 did not show improvement because the proposed method was unable to enhance the quality of the rPPG signal at the beginning of the video, as illustrated in Figure 8. This issue was caused by significant changes in ambient light conditions as noted by Sunkom et al. (2023). While the majority vote in subintervals method in improved HR values by extracting frequency components from reliable intervals, it did not yield similar improvements for PRV. This is likely because HR values can be accurately estimated from the good portions of the rPPG signal, whereas accurate PRV calculation requires the entire rPPG signal to be reliable.

For subject #35, the MAE results in Table 1 show that the values from both the conventional and proposed methods are notably similar. This suggests that the rPPG signal obtained using the conventional method was already of high quality.

Regarding SDPP, the MAE improved for all subjects, as shown in Table 2. Furthermore, the MAEs of RMSSD and SDSD improved for six of the seven subjects—specifically, subjects #5, #10, #14, #30, #32, and #35—as shown in Table 3 and Table 4.

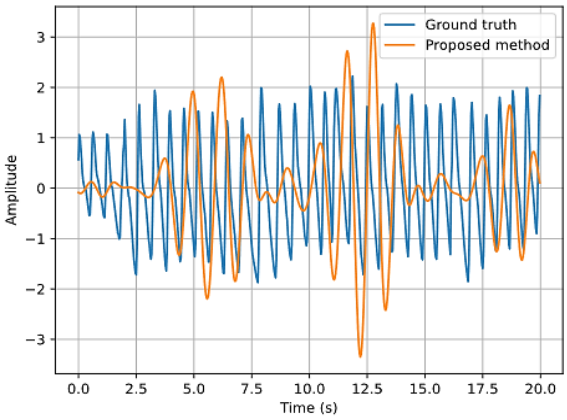

Figure 8. Failure of the proposed method to improve the rPPG signal of the subject #32 during the first interval of the video

4. CONCLUSION

This paper extended the prior research by applying the hair detection algorithm and the majority vote technique within subintervals—originally designed to improve HR—to the calculation of ultra-short-term PRV. The study utilized the rPPG signal extracted from the forehead ROI, incorporating modifications to the acquisition process to better accommodate PRV calculation and reduce complexity compared to previous methods. Evaluation of the MAE for various time-domain PRV features using the proposed method demonstrated noticeable improvements for most subjects compared to the conventional method. However, the proposed method was unable to enhance meanPP in cases where the video experienced significant fluctuations in ambient lighting.

Future research will focus on developing solutions to address the challenges identified in this study and further improving the accuracy of time-domain PRV. Additionally, potential improvement in the frequency domain using the proposed method will be explored.

ACKNOWLEDGMENTS

This research was supported by the Thailand Advanced Institute of Science and Technology and the Tokyo Institute of Technology (TAIST-Tokyo Tech) scholarship, a collaborative initiative between the National Science and Technology Development Agency (NSTDA), the Tokyo Institute of Technology, and Kasetsart University (KU).

REFERENCES

Aimie-Salleh, N., Ghani, N. A. A., Hasanudin, N., and Shafie, S. N. S. (2020). Heart rate variability recording system using photoplethysmography sensor. In *Autonomic Nervous System Monitoring - Heart Rate Variability* (Aslanidis, T., Ed.), pp. 29–44. London: IntechOpen.

Bobbia, S., Macwan, R., Benezeth, Y., Mansouri, A., and Dubois, J. (2019). Unsupervised skin tissue segmentation for remote photoplethysmography. *Pattern Recognition Letters*, 124, 82–90.

Bolanos, M., Nazeran, H., and Haltiwanger, E. (2006). Comparison of heart rate variability signal features derived from electrocardiography and photoplethysmography in healthy individuals. In *Proceedings of the 28th Annual International Conference of the IEEE Engineering in Medicine and Biology Society*, pp. 4289–4294. New York, USA.

de Haan, G., and Jeanne, V. (2013). Robust pulse rate from chrominance-based rPPG. *IEEE Transactions on Biomedical Engineering*, 60(10), 2878–2886.

Finžgar, M., and Podržaj, P. (2020). Feasibility of assessing ultra-short-term pulse rate variability from video recordings. *PeerJ*, 8, e8342.

Gudi, A., Bittner, M., and van Gemert, J. (2020). Real-time webcam heart-rate and variability estimation with clean ground truth for evaluation. *Applied Sciences*, 10(23), 8630.

Kartynnik, Y., Ablavatski, A., Grishchenko, I., and Grundmann, M. (2019). Real-time facial surface geometry from monocular video on mobile GPUs. *CVPR Workshop on Computer Vision for Augmented and Virtual Reality 2019*, Long Beach, CA, USA. [Online URL: https://arxiv.org/pdf/1907.06724v1] accessed on September 29, 2023.

Kumar, M., Veeraraghavan, A., and Sabharwal, A. (2015). DistancePPG: Robust non-contact vital signs monitoring using a camera. *Biomedical Optics Express*, 6(5), 1565–1588.

Lewandowska, M., Rumiński, J., Kocejko, T., and Nowak, J. (2011). Measuring pulse rate with a webcam — A non-contact method for evaluating cardiac activity. In *Proceedings of the 2011 Federated Conference on Computer Science and Information Systems*, pp. 405–410. Szczecin, Poland.

Makowski, D., Pham, T., Lau, Z. J., Brammer, J. C., Lespinasse, F., Pham, H., Schölzel, C., and Chen, S. H. A. (2021). NeuroKit2: A python toolbox for neurophysiological signal processing. *Behavior Research Methods*, 53(4), 1689–1696.

McCraty, R., and Shaffer, F. (2015). Heart rate variability: New perspectives on physiological mechanisms, assessment of self-regulatory capacity, and health risk. *Global Advances in Health and Medicine*, 4(1), 46–61.

Panigrahi, A., and Sharma, H. (2022). Non-contact HR extraction from different color spaces using RGB camera. In *Proceedings of the 2022 National Conference on Communications (NCC),* pp. 332–337. Mumbai, India.

Peng, R.-C., Zhou, X.-L., Lin, W.-H., and Zhang, Y.-T. (2015). Extraction of heart rate variability from smartphone photoplethysmograms. *Computational and Mathematical Methods in Medicine*, 2015(1), 516826.

Pinheiro, N., Couceiro, R., Henriques, J., Muehlsteff, J., Quintal, I., Gonçalves, L., and Carvalho, P. (2016). Can PPG be used for HRV analysis? In *Proceedings of the 38th Annual International Conference of the IEEE Engineering in Medicine and Biology Society (EMBC)*, pp. 2945–2949. Orlando, FL, USA.

Poh, M.-Z., McDuff, D. J., and Picard, R. W. (2010). Non-contact, automated cardiac pulse measurements using video imaging and blind source separation. *Optics Express*, 18(10), 10762–10774.

Pourbemany, J., Almabrok, E., and Zhu, Ye. (2021). Real-time video-based heart and respiration rate monitoring. In *Proceedings of NAECON 2021 - IEEE National Aerospace and Electronics Conference*, pp. 332–336. Dayton, OH, USA.

Ryu, J., Hong, S., Liang, S., Pak, S., Chen, Q., and Yan, S. (2021). Research on the combination of color channels in heart rate measurement based on photoplethysmography imaging. *Journal of Biomedical Optics*, 26(2), 025003.

Sanyal, S., and Nundy, K. K. (2018). Algorithms for monitoring heart rate and respiratory rate from the video of a user's face. *IEEE Journal of Translational Engineering in Health and Medicine*, 6, 2700111.

Sunkom, P., Worasawate, D., Srisurangkul, C., and Nakayama, M. (2023). Improved heart rate estimation from facial videos using hair detection and majority vote in subintervals. In *Proceedings of the 20th International Joint Conference on Computer Science and Software Engineering (JCSSE)*, pp. 380–384. Phitsanulok, Thailand.

Vescio, B., Salsone, M., Gambardella, A., and Quattrone, A. (2018). Comparison between electrocardiographic and earlobe pulse photoplethysmographic detection for evaluating heart rate variability in healthy subjects in short- and long-term recordings. *Sensors*, 18(3), 844.

Wang, W., den Brinker, A. C., Stuijk, S., and de Haan, G. (2017). Algorithmic principles of remote PPG. *IEEE Transactions on Biomedical Engineering*, 64(7), 1479–1491.

Yu, S.-G., Kim, S.-E., Kim, N. H., Suh, K. H., and Lee, E. C. (2021). Pulse rate variability analysis using remote photoplethysmography signals. *Sensors*, 21(18), 6241.